Modelling Fragmentation in Rock Avalanches

Øystein Thordén Haug, Matthias Rosenau, Karen Leever, and Onno Oncken

Abstract

The physical description of rock masses travelling down a slope is a complex problem, involving bouncing, rolling, sliding, flowing, fracturing and/or combinations of these. Modelling serves as a valuable tool to study these systems which are rarely monitored at high resolution in nature. Often, granular models (e.g. loose sand) are used to study rock avalanches in experimental simulations. For such granular models, one has to assume that the rock mass disintegrates instantaneously after detachment and that fragment size does not reduce further during the movement. We present a new method that overcomes this limitation by simulating dynamically fragmenting gravitational mass movements.

We have developed a material that fails in a brittle manner at lab scale conditions. The material is produced by cementing sand with gypsum (anhydrite) or potato starch, which allows controlling the shear strength over a wide range. Experiments are performed by releasing the material down a slope and monitoring with a digital camera at frequencies of 50 or 250 Hz. Two techniques are used to quantify the experimental results: particle image velocimetry which quantifies the surface velocity field, and optical image analysis to derive geometric (e.g. fragment size distribution) and mechanical properties (e.g. basal friction) of the model.

Preliminary results from the experiments illustrate the different dynamics of the gravitational mass movement as a function of shear strength.

Keywords

Rock avalanche • Fragmentation • Analogue material • Image analysis

Introduction

Rock avalanches are large (volume $>10^6$ m^3) rapid gravitational movements of rocks (Hsü 1975; Davies and McSaveney 1999). Rock-avalanche deposits are often made up of granular material with fragment sizes ranging from meter sized boulders down to dust on a micro-meter scale (Crosta et al. 2007; McSaveney and Davies 2007). The rock mass prior to the detachment can be assumed to have been more or less intact (Locat et al. 2006), suggesting that the deposits are the products of fragmentation processes occurring during detachment (static fragmentation) and during the travel (dynamic fragmentation).

Likely due to the shape and the granular nature of the deposits, rock avalanches are often modelled as granular flows both in analogue (Davies and McSaveney 1999; Iverson et al. 2004; Shea and van Wyk de Vries 2008; Dufresne 2012; Manzella and Labiouse 2012) and numerical (Campbell et al. 1995; Mollon et al 2012) experiments. However, using granular material to model rock avalanches means assuming that dynamic fragmentation is negligible, i.e., one assumes that the rocks instantaneously disintegrate

Ø.T. Haug (✉) • M. Rosenau • K. Leever • O. Oncken
Section 3.1—Lithosphere Dynamics, GFZ—Potsdam, Telegrafenberg, 14473 Potsdam, Germany
e-mail: thorden@gfz-potsdam.de; rosen@gfz-potsdam.de; karen.leever@gfz-potsdam.de; oncken@gfz-potsdam.de

K. Sassa et al. (eds.), *Landslide Science for a Safer Geoenvironment*, Vol. 2,
DOI 10.1007/978-3-319-05050-8_16,

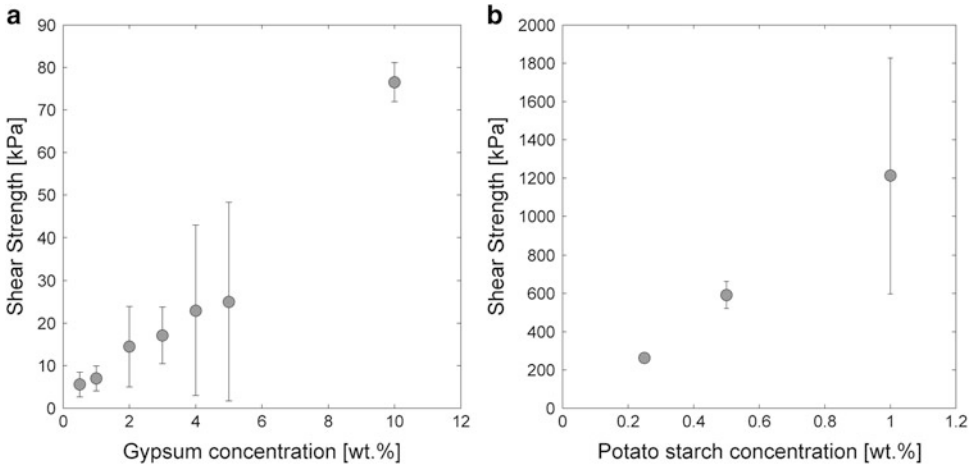

Fig. 1 Shear strength as a function of gypsum (**a**) and starch (**b**) concentrations. Each point is the mean value of 15 AT-tests and the error bars are given by the standard deviation around this mean

after detachment and that no further fragmentation occurs during the travel.

Few models have taken dynamic fragmentation during rock avalanches into consideration (Imre et al. 2010; Bowman et al. 2012) and these were performed in centrifuges, which pose restrictions on the possible scales that can be studied. Nevertheless, Bowman et al. (2012) showed that material that fragmented dynamically caused a longer runout than that of pre-fragmented material, suggesting that dynamic fragmentation is an important agent in rock-avalanche dynamics.

We study the effect of dynamic fragmentation in rock avalanches at lab scale under normal gravity conditions. To do this, a new rock-analogue material, and a method to quantitatively analyse the dynamics of fragmenting model avalanches have been developed. Compared to experiments performed in a centrifuge, this approach has the advantage that a wider range of scales can be studied and the potential to simulate more realistically the full process from detachment to deposition.

Analogue Material and Experimental Setup

According to the principle of model similarity (Hubbert 1937), the analogue material must behave in a dynamically similar way to the rocks in natural rock avalanches. Ideally, the material should therefore deform in a brittle manner with limited elastic and ductile strains up to a certain critical stress, beyond which the material breaks and deforms irreversibly.

The material is created by cementing together well-rounded fluvial quartz sand (average size ~300 μm) with a cementing agent. In the tests reported here, the cementing agents are gypsum (anhydrite) and potato starch (carbohydrate). The material properties are tested using a ring shear tester (RST) and a uniaxial tester (AT).

Material Preparation and Properties

The sand and the cement are first mixed while dry, afterwards a small amount of water (~10 wt%) is added and everything is thoroughly mixed to yield a homogeneous mass. The material is then placed inside a mould, and compacted by hammering by hand.

The material hardens by either setting for 48 h at room temperature (in the case of gypsum cement) or heating in a 900 W microwave oven for 15 min (in the case of potato starch cement).

The shear strength of the material can be controlled by the concentration of cementing agent. Systematic AT-tests of the effect of concentration shows that the shear strength can be varied between 1 and 10^3 kPa (Fig. 1). As seen in Fig. 1, the shear strength achieved using gypsum cement (hereafter called "g-cement", Fig. 1a) varies from 1 to 10^2 kPa and scales approximately linearly with the concentration. A stronger material can be achieved using potato starch cement (hereafter called "s-cement"). The correlation between the shear strength and the concentration of potato starch is also approximately linear and the shear strength of s-cement varies between 10^2 and 10^3 kPa (Fig. 1b). The two data sets (Fig. 1a, b) are seen to complement each other, allowing us to vary the shear strength over six orders of magnitude.

The frictional properties of a low strength material, g-cement$_{0.5}$ (lower case number referring to concentration, here 0.5 wt%), in comparison with loose sand, were tested using the RST (Fig. 2). Typical shear stress curves obtained from the RST are shown in Fig. 2a. In general, the shear

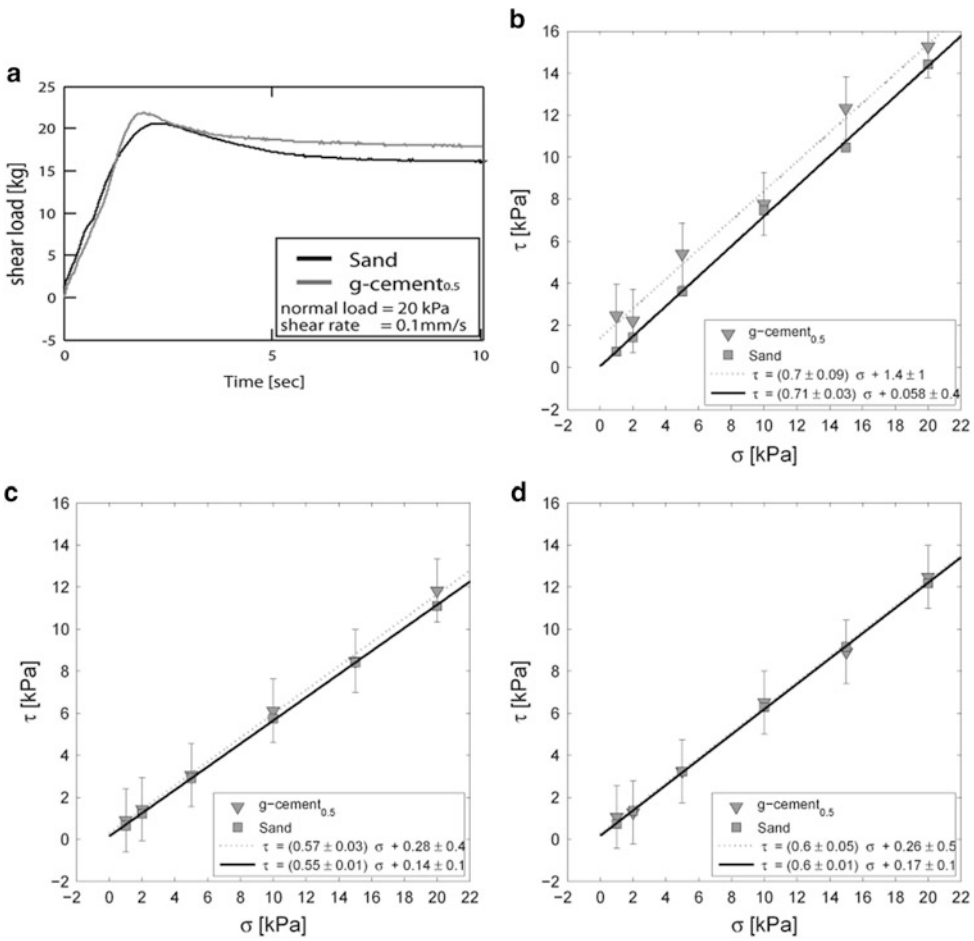

Fig. 2 Data from the ring shear tester (RST). (**a**) Raw data of sand and g-cement$_{0.5}$. (**b**)–(**d**) Comparisons of peak, kinetic and static friction between loose sand and g-cement$_{0.5}$

stress curves show an increase of shear stress until it reaches a peak (peak friction) when a shear fracture forms, followed by a decrease to a constant shear stress level (kinetic friction). A similar curve to that presented in 2a, but with a lower peak value, is obtained if a sample with an existing shear fracture is sheared (static friction).

In Fig. 2b, c, d, the results of a series of RST tests are presented. In these plots, the frictional strengths of g-cement$_{0.5}$ is compared with that of loose sand for normal stresses ranging from 0.5 to 20 kPa. The resulting linear relationships can be modelled as a Mohr-Coulomb failure envelope, the slope of which is the coefficient of friction and the y-axis intercept is the cohesion. Accordingly, the cohesion of undeformed loose sand is in the order of 10 Pa, while the cohesion of the g-cement$_{0.5}$ is in the order of 10^3 Pa (Fig. 2b). Importantly, the friction coefficients are not influenced by cementing, nor is there any residual cohesion once a fracture has been created (Fig. 2c, d). The peak static and kinetic coefficients of friction for both loose sand and the cemented sand are 0.7, 0.6 and 0.55, respectively.

We conclude that increasing concentration of cementing agent in the mix increases its primary cohesion, while the other frictional properties remain constant. Due to the small amount of cementing material, this is assumed for all concentrations.

Experimental Setup

In our setup, rock avalanches can be modelled at lab scale by a sudden release of material down a slope of 1–2 m length and at an angle of 30°–60°. Past the slope, the angle changes suddenly to 0° (Fig. 3). The experiments are monitored with a digital camera at frequencies of 50 and 250 Hz and image resolutions of 8.29 and 0.23 MPx, respectively.

Here we report the first series of experiments, consisting of three runs on a 45° dipping slope, where only the shear strength of the material is varied while all other parameters are kept constant. Materials used in this series are 1.5 kg samples of loose sand, g-cement$_{0.5}$ and s-cement$_1$. The shear strength thus varies from 10, 10^3 to 10^6 Pa (assuming shear

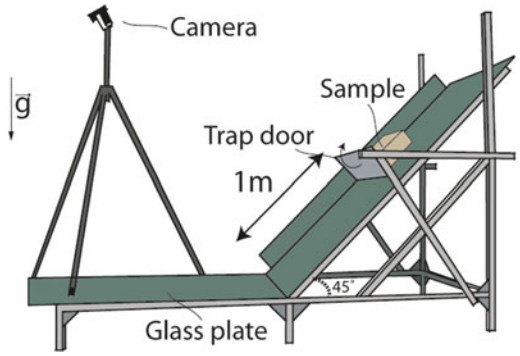

Fig. 3 Experimental setup

strength of sand ≈ cohesion of sand). The camera frequency during these experiments was 50 Hz at 8.29 MPx resolution.

The initial geometry of the released material is a rectangular cube of dimension 0.15 × 0.15 × 0.04 m^3 lying on its widest side. Additionally, a thin layer of red sand is added on top of the samples (not to the loose sand) to increase contrast for image analysis. The sliding base consists of glass plates.

Image Analysis

To quantify the experiments we use two types of image analysis: Particle Image Velocimetry (PIV) and Optical Image Analysis (OIA).

The goal of the image analysis is to measure deformation, velocity and fragmentation through time. The first two parameters are found using PIV, while the last point is found using OIA.

Before any analysis, the images are calibrated, i.e., corrected for distortions and the differences in distances between the different objects in the images and the camera. This is done using the PIV software (PIV Strainmaster by LaVision).

Particle Image Velocimetry

Particle Image Velocimetry (PIV) is used to monitor the velocity and deformation of the surface of the sliding material (Fig. 4a). The basic concept of the PIV method is to use cross-correlation of patterns in sequential images to detect the displacement of the pattern between the images (see Adam et al. (2005) for a comprehensive description).

The patterns in question are, in fact, a specific distribution of grayscale-intensities within a given interrogation window (a smaller part of the image). For the analysis given here the PIV-algorithm uses interrogation window sizes decreased from 256 × 256 to 128 × 128 pixels with 75 % overlap.

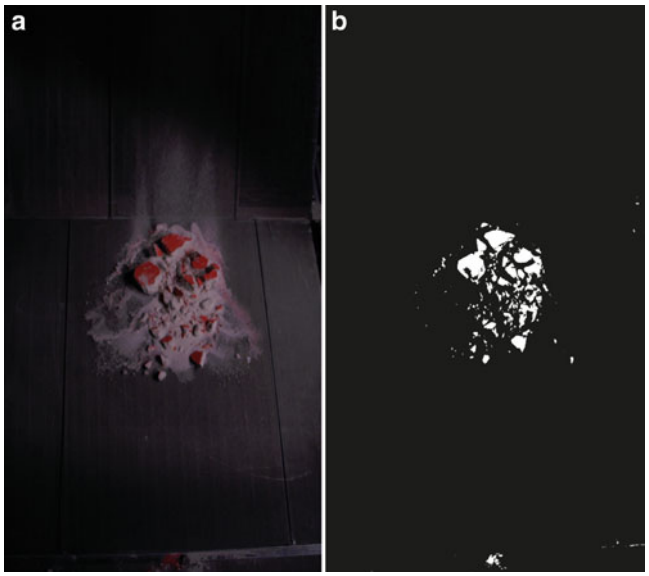

Fig. 4 (**a**) Example of an experimental image showing a fragmented block spreading on a horizontal plane. (**b**) Binary image of (**a**)

This results in velocity field resolution of 0.0563 m, at a precision of 0.03 m/s.

Optical Image Analysis

Optical Image Analysis (OIA) is used here to quantify the fragmentation process. The general strategy of OIA in our approach is to convert the original image (Fig. 4a) to a binary image (Fig. 4b) where the fragments are of value 1 (white) and everything else is of value 0 (black). In this process, all fragments below a size of 10 pixels are considered background. The binary image is created in three steps. In each step a binary image is produced, and in the end all these are combined into one final binary image (Fig. 4b).

The first binary image is produced by considering only the red contribution to the RGB image. The image is binarized by setting all pixels with intensity above a certain limit to 1 and all below to 0. This process is called thresholding. Since the top of the samples have a thin layer of red sand (see Fig. 4a), this procedure captures most of the larger fragments which have not rotated. The second binary image is produced by converting the RGB image to grayscale and thresholding it. This method is most appropriate to find the largest fragments. The third binary image is found by differentiating in both directions across the grayscale image, subtracting this from the original grayscale image, and thresholding the resulting image. This procedure finds the small fragments, and is also capable of extracting fragments which are resting on top of sand (which is considered background).

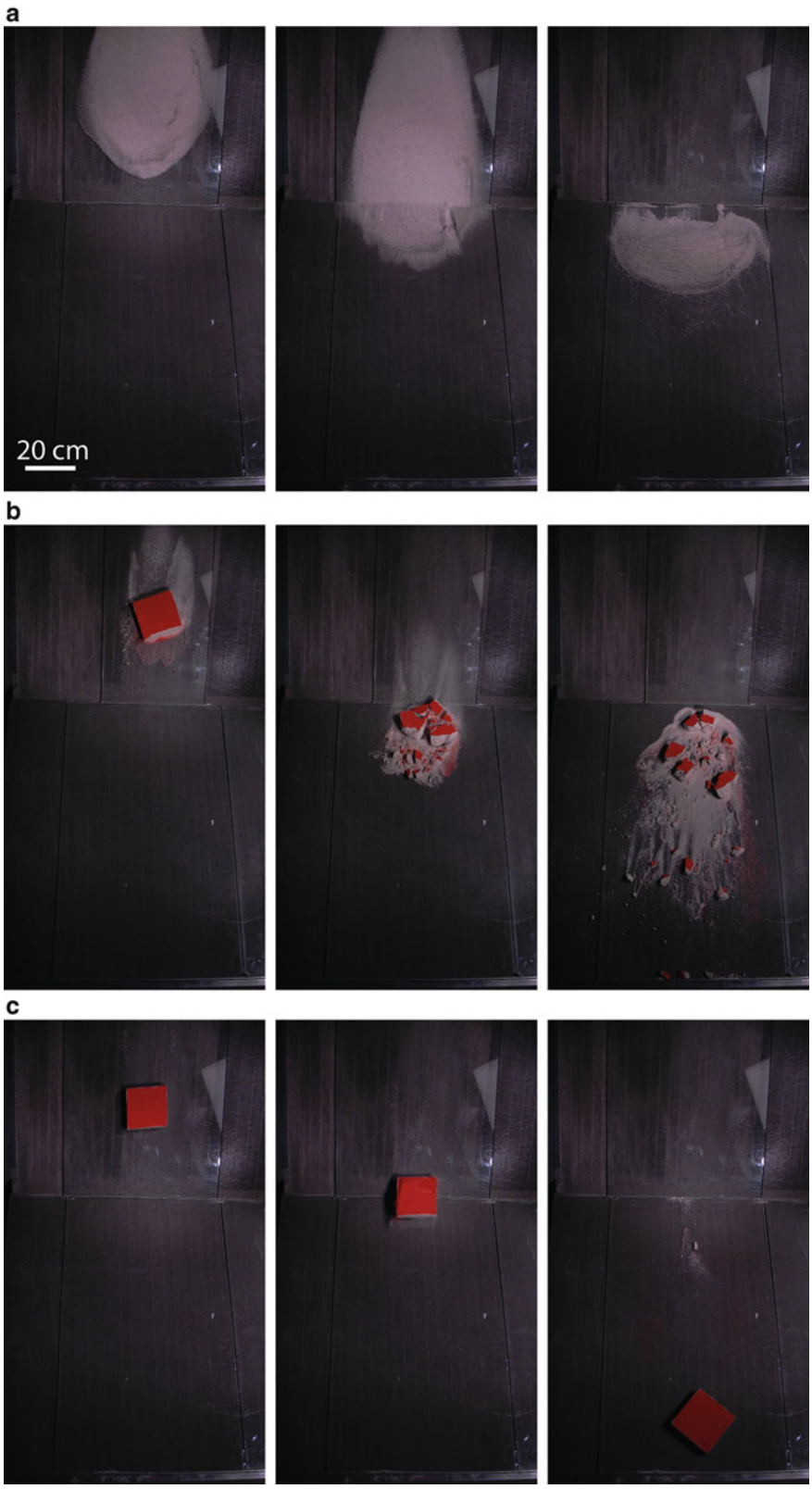

Fig. 5 Images of experiments with different cohesion (**a**) loose sand (SS = 10^1 Pa), (**b**) g-cement$_{0.5}$ (SS = 10^3 Pa), and (**c**) s-cement$_1$ (SS = 10^6 Pa)

The sizes of the fragments are approximated by the areas they project on the images and are given in equivalent diameters.

$$L = \sqrt{\frac{Area}{\pi}}$$

Additional to the fragmentation process, OIA is used to monitor the area covered by the slide through time. In this calculation, the area is found by considering all fragment sizes. In practice, this is done by thresholding so that all the sand and blocks are 1's while the rest is 0.

Preliminary Observations and Interpretation

Figure 5 shows snapshots of three different experiments, where the shear strength (SS) is varied from 10 (Fig. 5a), 10^3 Pa (Fig. 5b) to 10^6 Pa (Fig. 5c). All other parameters are kept constant. The sand, in Fig. 5a, can be described as flowing, in contrast, the block in Fig 5c is sliding. The fragmenting block (Fig. 5b) is at first seen to slide, until it hits the knickpoint, at which point it breaks and spreads across the horizontal plane. The longest runout is seen for the intact block, and the second longest for the fragmenting block, while the loose sand shows the shortest runout. This may reflect the difference in energy consumption due to internal deformation which is lowest for the intact block.

PIV-derived velocity fields of the experiments from Fig. 5a, b is presented in Fig. 6. These show that the behaviour of the two experiments is kinematically different on the horizontal plane: While the loose sand avalanche has higher displacement in the rear than in the front of the pile, the cement slide-avalanche has higher displacement in the front than in the rear. This suggests that the material in the sand avalanche actively contracts while the g-cement$_{0.5}$ avalanche expands, in the direction of travelling.

The evolutions of areas of the slides are presented in Fig. 7a and shed light on the role of basal contact area on runout. The vertical line represents the time when the material reaches the horizontal plane. For the experiment with SS = 10^1 Pa (Fig. 5a) the area is seen to increase until ca. 0.2 s after reaching the plane, after which the area decreases again. This behaviour reflects the active spreading and contraction during movement of the avalanche. For the experiment shown in Fig. 5b (SS = 10^3 Pa) an initial increase is seen, until a plateau is reached, the area increases again directly after impact. The first increase is due to the sample moving into the field of view, while the second reflects the spreading after fragmentation. For the experiment shown in Fig. 5c (SS = 10^6 Pa) the area is seen to be more or less constant, reflecting the rigid block-like behaviour of the slide. Considering the differences in runout, one might argue that the frictional energy dissipation is more pronounced for low-cohesive material due to (a) the increase of basal sliding area during acceleration in combination with (b) frictional dissipation by compressive internal deformation during deceleration.

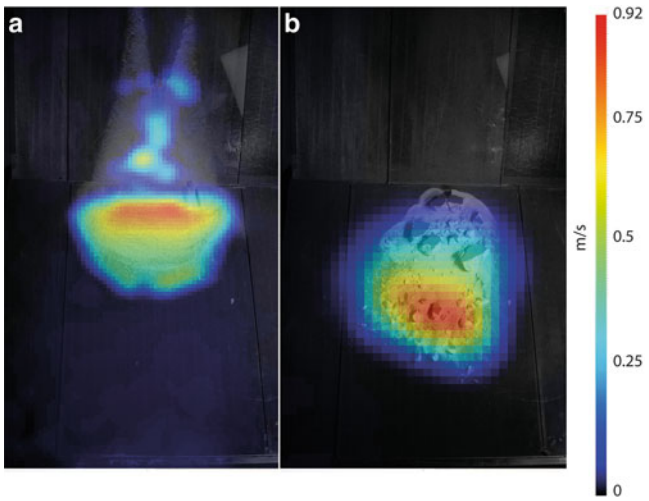

Fig. 6 Snapshots of the velocity field calculated from the PIV for experiments shown in Fig. 5a (**a**) and 5b (**b**)

In Fig. 7b snapshots of the fragment size distribution (FSD) are presented. The approximately linear trends of the fragment size distributions suggest that they can be described by power-laws where the exponent is given by the slope. Interestingly, the slopes of the fragment size distributions appear more or less constant through time, while the distribution is shifted towards higher numbers in time. This suggests that the fragmentation is a self-organized (fractal) process.

Discussion

Limitations of the Approach

From Fig. 1, it is observed that that the uncertainty of the shear strength (SS) increases with the strength, reflecting the variability of the sample material under otherwise identical preparation conditions. Most likely, this variability in shear strength arises because the material is not completely homogenous. One might therefore expect the fragmentation to be affected by the variability of the material and should not

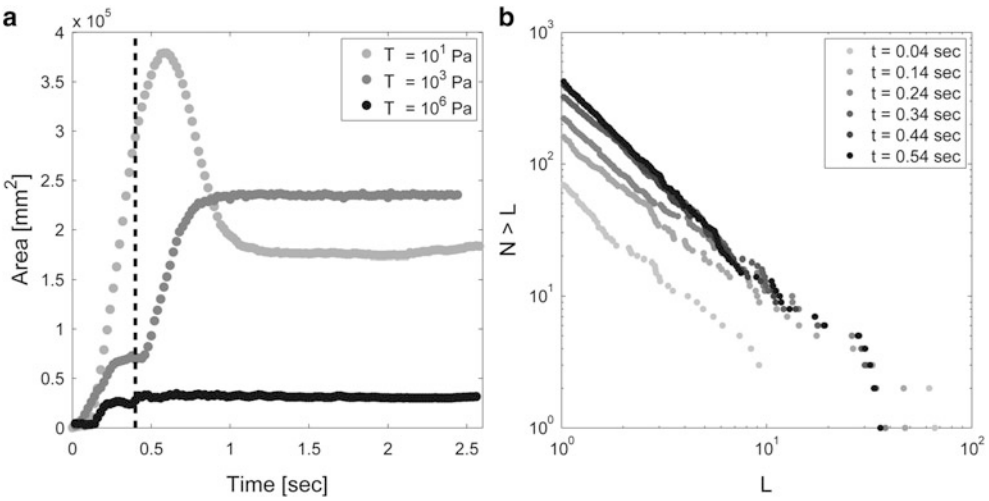

Fig. 7 (**a**) Basal area during slide for the three experiments shown in Fig 5. Vertical line displays time of impact. (**b**) Fragment size distribution (FSD) at different time steps for the experiment presented in Fig 5b. Time given in legend is after impact

over-interpret single experiments. Instead, a large number of experiments are needed to constrain uncertainty of experimental results.

Even though the OIA finds fragments and their sizes, there are some problems related to this approach. One is that sometimes piles of sand may be interpreted as fragments, even though they should not be. This error is minimized by removing fragments with very elongated shapes. A second problem is that shadows can cause separation of larger fragments into several smaller ones. This effect is dealt with by averaging over time. The OIA only takes into account fragments larger than 10 pixels, equivalent to a 4.4 mm long fragment. A rough estimate of how much material is below this level can be found by comparing the total area of all fragments registered and the total are of the entire slide. Such an estimate for the experiment presented in Fig. 5a suggests that the latter is as much as 1 order of magnitude larger. This can cause a bias of the fragment size distribution to the coarser end of the distribution. However, if the fragment size distributions truly are scale-invariant power laws, the exponent should remain the same regardless of the resolution.

Comparison with Centrifuge Models

Similar to what Bowman et al. (2012) showed, we also see that a fragmenting material travels further than a pre-fragmented one (Fig. 5a, b), corroborating their interpretation that fragmentation can be viewed as an energy source. Our results show, however, that an even longer runout is achieved for an intact block. This may suggest that dynamic fragmentation causes loss of cohesion, which causes higher energy dissipation due to increased internal deformation and larger basal friction (due to increased basal area).

Imre et al. (2010) found that their experimental fragment size distribution was given by power laws and interprets this to be due to a fractal process. Our experimental fragment size distributions are also well approximated by power laws. However, a linear regression of the data in Fig. 7b reveals a power law exponent of ~1 $\pm$ 0.2, this is steeper than the ~0.4 exponent found by Imre et al. (2010). Such a discrepancy might be caused by our bias toward larger fragments. Imre et al. also report a steeper slope for the larger fragments.

Conclusion and Outlook

We have developed a tool for studying fragmentation in rock avalanches. Rock avalanches are modelled at lab scale by releasing an analogue material down a slope. The shear strength of the material can be controlled by the amount of cementing agent added to the sand. Our image analysis tool allows us to quantify the fragmentation process and the following dynamics of the slide.

With this new tool, we plan to perform a parameter study, to better understand the changes in dynamics and energetics of a system of varying shear strength.

Acknowledgments Thanks to Frank Neumann and Thomas Ziegenhagen for construction and technical assistance. The work is supported by GEOSIM and BMBF.

References

Adam J, Urai JL, Wieneke B, Oncken O, Pfeiffer K, Kukowski N, Lohrmann J et al (2005) Shear localisation and strain distribution during tectonic faulting—new insights from granular-flow experiments and high-resolution optical image correlation techniques. J Struct Geol 27(2):283–301

Bowman ET, Take WA, Rait KL, Hann C (2012) Physical models of rock avalanche spreading behaviour with dynamic fragmentation. Can Geotech J 49(4):460–476

Campbell CS, Cleary PW, Hopkins M (1995) Large-scale landslide simulations: global deformation, velocities and basal friction. J Geophys Res 100(B5):8267–8283

Crosta GB, Frattini P, Fusi N (2007) Fragmentation in the Val Pola rock avalanche, Italian Alps. J Geophys Res 112:F01006

Davies TR, McSaveney M (1999) Runout of dry granular avalanches. Can Geotech J 36(2):313–320

Dufresne A (2012) Granular flow experiments on the interaction with stationary runout path materials and comparison to rock avalanche events. Earth Surf Proc Land 37(14):1527–1541

Hubbert M (1937) Theory of scale models as applied to the study of geologic structures. Geol Soc Am Bull 48(October): 1459–1520

Hsü KJ (1975) Catastrophic debris streams (sturzstroms) generated by rockfalls. Geol Soc Am Bull 86(50117):129–140

Imre B, Laue J, Springman SM (2010) Fractal fragmentation of rocks within sturzstroms: insight derived from physical experiments within the ETH geotechnical drum centrifuge. Granul Matter 12(3):267–285

Iverson RM, Logan M, Denlinger RP (2004) Granular avalanches across irregular three-dimensional terrain: 2 experimental tests. J Geophys Res 109, F01015

Locat P, Couture R, Leroueil S, Locat J, Jaboyedoff M (2006) Fragmentation energy in rock avalanches. Can Geotech J 43(8)

Manzella I, Labiouse V (2012) Empirical and analytical analyses of laboratory granular flows to investigate rock avalanche propagation. Landslides 10(1):23–36

McSaveney MJ, Davies T (2007) Rockslides and their motion. In: Sassa K, Fukuoka F, Wang F, Wang G (eds) Progress in landslide science. Springer, Berlin, pp 113–133

Mollon G, Richefeu V, Villard P, Daudon D (2012) Numerical simulation of rock avalanches: influence of a local dissipative contact model on the collective behavior of granular flows. J Geophys Res 117(F2): 1–19

Shea T, van Wyk de Vries B (2008) Structural analysis and analogue modeling of the kinematics and dynamics of rockslide avalanches. Geosphere 4:657–686